05,13

Influence of elastic strains on the dipole spin wave spectrum in the lateral system of magnonic crystals with a piezoelectric layer

© A.A. Grachev[1], M. Mruczkiewicz[2], E.N. Beginin[1], A.V. Sadovnikov[1]

[1] Saratov National Research State University,
Saratov, Russia
[2] Institute of Electrical Engineering, Slovak Academy of Sciences, Dúbravská cesta 9,
841 04 Bratislava, Slovakia

E-mail: stig133@gmail.com

Received April 29, 2022
Revised April 29, 2022
Accepted May 12, 2022

In this work, we will reveal the regularities in the control of the dipole spin-wava spectra of in lateral heterostructures formed from two magnonic crystals with a piezoelectric layer placed on one of them. The electric field control of the spatial and transfer characteristics of dipole spin waves in lateral heterostructures is shown. Based on the finite element method, the influence of distributed elastic deformations on the magnitudes of internal magnetic fields in magnonic crystals is evaluated. Based on the results of numerical simulations, a physical interpretation of the transformation of the eigenmode spectrum of coupled magnon crystals is given.

Keywords: spin waves, magnonics, straintronics, lateral structures.

DOI: 10.21883/PSS.2022.09.54176.45HH

1. Introduction

Recent advances in micro- and nanoscale magnetic structures based on insulating materials offer a promising alternative to spin wave (SW) signal processing over CMOS (complementary metal–oxide–semiconductor) technologies, based on magnonic networks [1,2] increasing the functionality of elementary nodes in computing systems, and having low power consumption. Micro- and nanoscale magnetic structures act as a promising base for creating magnonic integrated circuits [3,4], overcoming the limitations of CMOS electronics [5]. In this case, the main attention is paid to the use of SW as carriers of information signals, because in this case it is possible to implement a number of signal processing devices on the principles of magnonics [1,5].

Over the past few years, periodic magnetic structures, magnonic crystals (MCs), have become the subject of considerable interest in the scientific community because of the possibility of creating predetermined SW transmission properties [1,6–8]. One of the main reasons for studying MCs at present is their promising application to create logic systems [2,7] using the wave nature of spin excitations. On the other hand, lateral ferrite structures attract wide attention of researchers because of the possibility of their use as multichannel signal processing systems in nanoscale based on the principles of magnonics [7,9]. In the signal transmission system based on two ferrite micro waveguides with an air gap between them, the interference of symmetric and antisymmetric forms is observed, which manifests itself in a periodic redistribution of the signal between the microwaves [10,11]. At present, research on the possibility of controlling the spectrum of spin waves in ferrite micro waveguides through the influence of distributed elastic deformations on the ferrite [12–16] layer is being actively pursued.

The present work reveals patterns of dipole spin wave spectrum control in lateral heterostructures formed from two magnon crystals with a piezoelectric layer placed on one of them. Electrical field control of the spatial and transmission characteristics of dipole spin waves in lateral heterostructures is demonstrated. Based on the finite element method, the effect of distributed elastic deformations on the magnitudes of internal magnetic fields in magnonic crystals is evaluated. Based on the results of numerical simulations, a physical interpretation of the phenomenon of transformation of the spectrum of eigenmodes of coupled magnonic crystals is given.

2. Structure and numerical study

Consider the structure shown in Fig. 1. The system is a parallel-oriented magnetic micro waveguides, with the width of $w = 500\,\mu$m and distance between them $d = 40\,\mu$m made using the method of laser scribing from a single-crystal ferrite YIG film with a thickness of $10\,\mu$m with saturation magnetization $M_0 = 139$ G. Two magnetic micro waveguides are located on the same substrate of GGG, $200\,\mu$m thick. The length of the first magnetic micro waveguide (MC1) was $L_1 = 7$ mm, and the second (MC2) was $L_2 = 4$ mm. A system of periodic grooves with a period of $L = 200\,\mu$m is formed on the surface of both magnetic microwaves, forming a MC. The groove depth was $1\,\mu$m. A $200\,\mu$m thick PZT layer, located on one of the MCs, was

used as the piezoelectric material. A 1 μm thick titanium electrode was placed on the top side of the PZT layer, which has no significant effect on the propagation of spin waves in the magnonic crystal. There is a titanium electrode with a thickness of 100 nm on the bottom side of the PZT. The structure was placed in an external static magnetic field $H_0 = 1200$ Oe in the direction of x axis for efficient excitation of magnetostatic surface waves (MSSW).

A numerical model based on the finite element method (FEM) [17,18] was developed to describe the physical processes that determine the physical characteristics of spin-wave signal control by creating local elastic deformations. In the first stage, we calculated the elastic deformations caused by an external electric field in the piezoelectric layer. Next, the internal magnetic field profiles in MC were calculated. The obtained internal magnetic field profiles were then used in micromagnetic simulations [19]. In the stage of solving the magnetostrictive problem, it was assumed that the magnetostrictive effect can be modeled using linear coupled equations if the material response consists of small deviations from the position of the operating point (displacement point), with the relationship between the mechanical stress **S**, the magnetic field **H** and the magnetic flux density **B** expressed as

$$\begin{cases} \mathbf{S} = c_H \varepsilon - e_{HS}^T \mathbf{H}, \\ \mathbf{B} = e_{HS} \varepsilon + \mu_0 \mu_{rS} \mathbf{H}, \end{cases}$$

where μ_0 — magnetic permeability of free space, and μ_{rS} — relative magnetic permeability at constant strain; e_{HS} — piezomagnetic coupling matrix (sign „T“ means transpose operation); ε — strain matrix. In this case, the voltage in the magnetostrictive material is described by the relation:

$$\mathbf{S} = c_H \left[\varepsilon_{el} - \varepsilon_{me}(\mathbf{M}) \right],$$

where the stiffness matrix c_H is defined by two parameters: the Young modulus ($E = 2 \cdot 10^{12}$ Pa) and the Poisson ratio $\nu = 0.29$. The relation for magnetostrictive strain ε_{me} is expressed as a quadratic isotropic function of magnetization **M**:

$$\varepsilon_{me} = \frac{3}{2} \frac{\lambda_S}{M_s^2} \operatorname{dev}(\mathbf{M} \otimes \mathbf{M}),$$

where the tensor product of the two vectors is defined as $(\mathbf{M} \otimes \mathbf{M})_{ij} = M_i M_j$, and $\lambda_S = -2.2 \cdot 10^{-6}$ — saturation magnetostriction, which is the maximum magnetostrictive strain achieved at saturation magnetization M_0. Note that the magnetostrictive strain is represented by a deviatoric tensor. This is due to the fact that the deformation can be associated with the rotation of the magnetic domain, while such a process should not change the volume of the material.

The nonlinear magnetization in a magnetostrictive material is found from the following nonlinear implicit relation

$$\mathbf{M} = M_0 \mathrm{L}(|\mathbf{H}_{\text{eff}}|) \frac{\mathbf{H}_{\text{eff}}}{|\mathbf{H}_{\text{eff}}|},$$

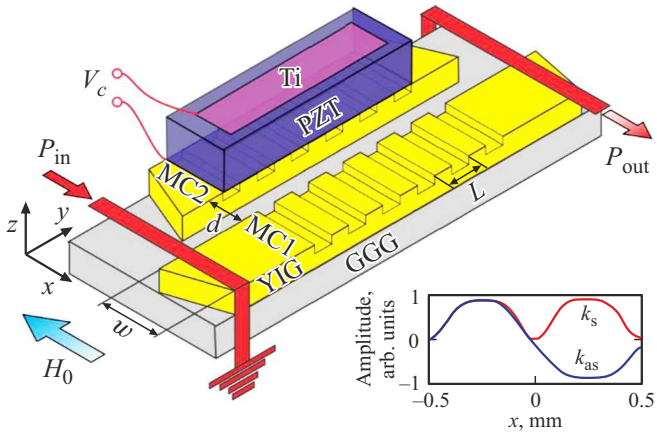

Figure 1. The diagram of the considered structure consisting of two lateral magnon-crystalline microwaves with an air gap. The bottom left inset shows the transverse profiles for the symmetric (k_s) and antisymmetric (k_{as}) eigenmodes of the lateral MC.

where L — the Langevin function, and represented as

$$\mathrm{L} = \operatorname{cth}\left(\frac{3\chi_m |\mathbf{H}_{\text{eff}}|}{M_0} - \frac{M_0}{3\chi_m |\mathbf{H}_{\text{eff}}|}, \right)$$

where χ_m — magnetic susceptibility in the initial linear region. For cubic crystals, the effective field in the material is determined by the expression

$$\mathbf{H}_{\text{eff}} = \mathbf{H}_0 + \frac{3}{\mu_0 M_0^2} \Big[\lambda_{100} \mathrm{S}_{\text{ed}} + (\lambda_{111} - \lambda_{100}) \times \sum_{i \neq j} (\mathrm{S}_{\text{ed}})_{ij} (\mathbf{e}_i \otimes \mathbf{e}_j) \Big] \mathbf{M},$$

where $\mathbf{H}_0$ — the applied magnetic field. The second term in this equation represents the contribution of mechanical stress to the effective magnetic field and hence to the magnetization of the material, which is called the Villari effect. The deviatoric stress tensor is related to the strain as: $\mathrm{S}_{\text{ed}} = \operatorname{dev}(c_H \varepsilon)$. In addition, magnetization and magnetic field are related to each other and to the magnetic flux density by the relationship: $\mathbf{B} = \mu_0(\mathbf{H}_0 + \mathbf{M})$.

Fig. 2, *a* shows the distribution of the mechanical stress modulus in the case of applying a positive electric field to the PZT layer. It can be seen that the deformation of the piezoelectric layer occurs in the area of the electrode, which, due to the reverse piezoeffect, is transferred to the YIG film, which in turn also deforms. Because of the inverse magnetostriction effect, the internal magnetic field in the MC changes. Next, the effect of piezoelectric layer deformation on the internal magnetic field of the magnonic crystal was evaluated. In these calculations, the following magnetostrictive constants were used for the YIG film at room temperature: $\lambda_{100} = -1.4 \cdot 10^{-6}$ and $\lambda_{111} = -2.4 \cdot 10^{-6}$, equal to the relative magnetostrictive elongation along the respective axes x and z. Fig. 2, *b* shows the distribution of

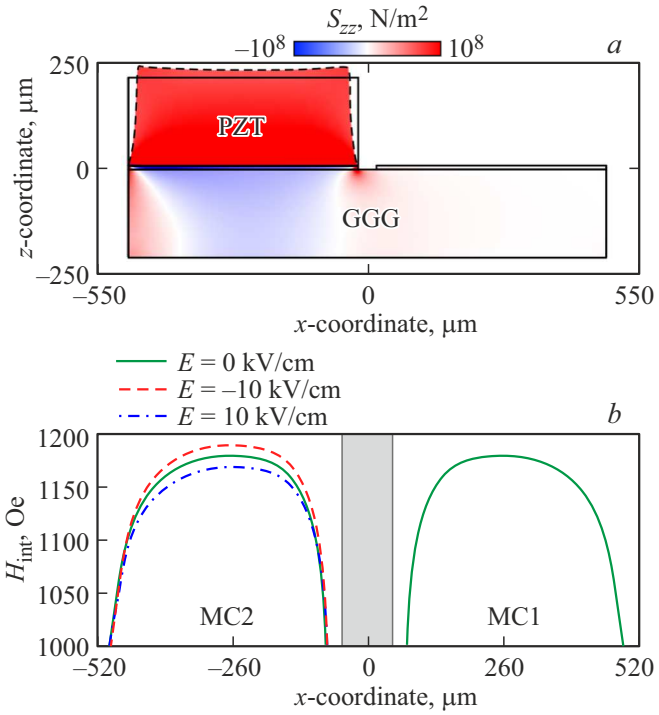

Figure 2. (a) Distribution of the mechanical stress tensor components S_{ZZ} when an external electric field $E = -10$ kV/cm is applied to the PZT layer. (b) Internal magnetic field profiles H_{int} in cases $E = 0$ kV/cm (solid green curves), $E = 10$ kV/cm (dashed blue curve), $E = -10$ kV/cm (dashed red curve) External magnetic field value in all cases was $H_0 = 1200$ Oe.

the internal magnetic field along the widths of the magnonic crystals at an external electric field of $E = 0$ kV/cm (green solid curves), $E = 10$ kV/cm (dashed blue curve) and $E = -10$ kV/cm (red dashed curve). It is worth noting that the effective control of the SW properties propagating in the lateral structure by means of local elastic deformations is possible due to the inhomogeneous distribution of the value H_{int}. When the magnetic field H_0 is directed along the x axis, the distribution of $H_{int}(x)$ in lateral MCs becomes non-uniform due to shape anisotropy, resulting in the formation of two spin-wave channels along which SWs propagate (see Fig. 2, b). Applying a positive (negative) electric field to the electrode leads to a decrease (increase) of the internal magnetic field in the second magnonic crystal (MC2), as shown in Fig. 2, b. It is worth saying that the inequality of the internal magnetic fields in lateral MCs leads to a transformation of the dynamics of SW propagation in such a system.

Further, micromagnetic modeling based on the finite difference method in the time domain was used to demonstrate the processes of SW generation and propagation in the system in question, as well as to control the spin-wave transport by means of distributed elastic deformations. Free software code mumax[3] supporting CUDA parallel computing technology was used. This method is based on the numerical solution of the Landau–Lifshitz–Gilbert (LLG) equation [20,21]. The computational domain was divided into a grid with the following element size: $1.95 \times 2 \times 1\,\mu m^3$.

To calculate the dispersion characteristics of spin waves propagating in a system formed of two lateral magnonic crystals, the signal in the input section of one of the magnonic-crystal micro waveguides was set in the form $h_z(t) = h_0 \sin c(2\pi f_c t)$, the central frequency $f_c = 7$ GHz, $h_0 = 0.1$ Oe. To plot the dispersion characteristic of spin waves in the numerical simulation, we calculated the value of

$$D(k_y, f) = \frac{1}{N}\sum_{i=1}^{N} |\Theta_2[m_z(x_i, y, t)]|^2,$$

where Θ_2 — two-dimensional Fourier transform operator, x_i — i-th cell and $N = 256$ — number of cells along the width of the magnonic crystal.

The two-dimensional distribution of $D(k_y, f)$ is color coded in Fig. 3, a, b. On the plane (f, k_y), it is possible to identify the set of points corresponding to the maximum of $D(k_y, f)$ value, which represent the dispersion characteristics of the symmetric and antisymmetric spin-wave form, labeled in Fig. 3, a, b, as k_s and k_{as}, respectively. It should be noted that the eigenmode spectrum of two identical lateral micro waveguides consists of symmetric and antisymmetric transverse forms (see the inset in Fig. 1). For the symmetric form, in the x-axis direction, the amplitudes of the magnetic potentials in two YIG films have the same phase (along the x-axis), while for the antisymmetric mode they are in antiphase by π. Also in the system, in the region of the Bragg wavelength constant $k_B = \frac{\pi}{L} = 157\,cm^{-1}$, where L — period of the magnonic crystal, the formation of non-transmission bands and forbidden zones in spin wave spectra are observed, which can be seen from the calculated dispersion characteristics. In this case, near the frequency of 5.35 GHz you can see (see Fig. 3, a) the formation of the forbidden zone, both for symmetric and antisymmetric modes of lateral structure. This effect can be explained by the mechanism of splitting of the Bragg forbidden zone and the formation of twin zones of signal non-passing in the system of two lateral MCs. In this case, the low-frequency forbidden zone corresponds to the antisymmetric form band, while the high-frequency forbidden zone — to the symmetric form band [10,22]. It should be noted that in this type of lateral structures, where the coupling between the waveguide structures is carried out by dynamic magnetic fields in the region of the side walls of the micro waveguides, it is possible to transfer spin-wave energy between micro waveguides [10]. With the help of the plotted dispersion characteristic we can estimate the SW coupling length parameter (L_c), which is numerically equal to the distance at which the complete power transfer from the first to the

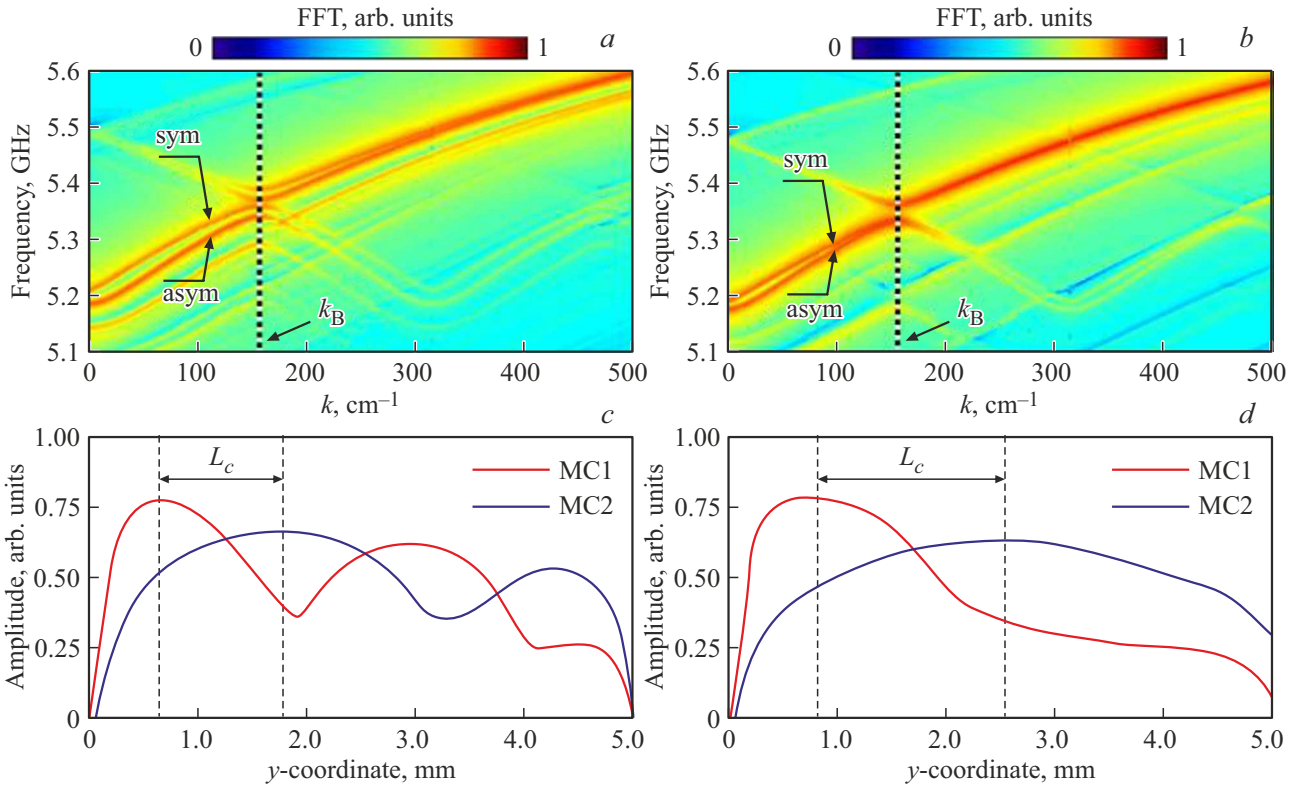

Figure 3. Dispersion characteristics of two lateral magnonic crystals at $E = 0$ kV/cm (a) and $E = 10$ kV/cm (b), obtained by micromagnetic simulation. Spatial spin-wave intensity distributions calculated by micromagnetic simulations at $f = 5.45$ GHz (c) and $f = 5.35$ GHz (d).

second MC takes place. In this case, the coupling length is defined as

$$L_c(f) = \frac{\pi}{|k_s(f) - k_{as}(f)|},$$

where $k_s(f)$ and $k_{as}(f)$ — the wavelength constants of the symmetric and antisymmetric forms. In this case, the left panels show the case of $E = 0$ kV/cm, and Fig. 3, b is the case $E = 10$ kV/cm. It can be seen that at $E = 10$ kV/cm in the system there is a narrowing of the branches of symmetric and antisymmetric forms, and, therefore, closure of one of the Bragg forbidden zones. This effect can be explained by the inequality of the internal magnetic fields in magnonic crystals and, as a consequence, the transformation of the spectrum of eigenmodes and the inequality of dispersions in each MC. At the same time, we can conclude that in the lateral system in question the MCs cease to be identical.

Fig. 3, c, d shows the longitudinal distribution of the value of m_z squared component of the dynamic magnetization at $f = 5.455$ GHz (in long-wave part of the spin-wave spectrum) and at the frequency of the forbidden zone, respectively. There is a periodic exchange of spin-wave power between MC. It should be noted that at the frequency of the forbidden zone the wave propagates mainly along the second MC. At the same time, Fig. 3, (c, d) demonstrates that the SW power is transferred from one MC to another in a periodic manner. In Fig. 3, c, d the L_c coupling length value is marked, when falling on the frequency of the forbidden zone in the system there is a sharp increase L_c, and the effect of elastic deformations allows to control the position of the forbidden zone. Thus, using the proposed mechanism for controlling the spectrum of eigenmodes in a lateral magnonic-crystal structure, one can perform spatial-frequency selection of the spin-wave signal. In this case, the power of the wave excited in one of the micro waveguides can be redistributed between the magnonic-crystal micro waveguides in a controlled manner due to changes in the coupling between the structures due to elastic deformations. In the vicinity of the frequency band of non-penetration caused by wave reflection from a periodic system of grooves inside each of the micro waveguides, the effect of elastic deformations on the positions of the frequency boundary of the Bragg forbidden zone is most strongly manifested when one of the magnonic crystals is deformed.

3. Conclusion

Thus, the regularities of controlling the spectrum of dipole spin waves in a heterostructure formed by a system of magnonic crystals with a piezoelectric layer rigidly connected to one of them were revealed. Based on the finite element method, a three-dimensional model of a

lateral system of magnonic crystal micro waveguides with a piezoelectric layer is constructed and the transformation of the magnitude of the internal magnetic field in the magnonic crystal is demonstrated when the magnitude and polarity of the external electric field applied to the piezoelectric layer change. With the help of micromagnetic modeling the problem of excitation and propagation of a spin wave in a lateral structure was solved. The longitudinal distributions of the orthogonal surface square of the micro waveguide projection of dynamic magnetization in the multiferroic structure under the variation of the shape of the internal magnetic field profile caused by the inverse magnetostriction effect are obtained, and the frequency shift of the Bragg forbidden zone gap with a change in the external electric field value is shown. With the help of micromagnetic modeling, the eigenmode spectrum was analyzed and the dispersion characteristics of the lateral structure were plotted. Numerical analysis reveals a frequency shift and a change in the width of the Bragg forbidden zones, and there is a closure of one of the forbidden zones. The proposed system of magnonic crystal microwaves can be used as a spatial-frequency filter of the information signal.

Funding

The study was performed with the support of the Ministry of Education and Science of Russia under the Government Task (project No. FSRR-2020-0005).

Conflict of interest

The authors declare that they have no conflict of interest.

References

[1] S.A. Nikitov, A.R. Safin, D.V. Kalyabin, A.V. Sadovnikov, E.N. Beginin, M.V. Logunov, M.A. Morozova, S.A. Odintsov, S.A. Osokin, A.Yu. Sharaevskaya, Yu.P. Sharaevskiy, A.I. Kirilyuk. UFN, **63**, 945 (2020) (in Russian).
[2] A. Khitun, M. Bao, K.L. Wang. J. Phys. D **43**, 264005 (2010).
[3] Y. Haiming, O. Kelly, V. Cros, R. Bernard, P. Bortolotti, A. Anane, F. Brandl, F. Heimbach, D. Grundler. Nature Commun. **7**, 11255 (2016).
[4] A.V. Sadovnikov, C.S. Davies, V.V. Kruglyak, D.V. Romanenko, S.V. Grishin, E.N. Beginin, Y.P. Sharaevskii, S.A. Nikitov. Phys. Rev. B **96**, 060401(R) (2017).
[5] A. Barman, G. Gubbiotti, S. Ladak, A.O. Adeyeye, M. Krawczyk, J. Gräfe. J. Phys.: Condens. Matter **33**, *41*, 413001 (2021).
[6] S.A. Nikitov, P. Tailhades, C. Tsai. J. Magn. Magn. Mater. **236**, *3*, 320 (2001).
[7] A.V. Chumak, A.A. Serga, B. Hillebrands. J. Phys. D **50**, *24*, 244001 (2017).
[8] P. Frey, A.A. Nikitin, D.A. Bozhko, S.A. Bunyaev, G.N. Kakazei, A.B. Ustinov, B.A. Kalinikos, F. Ciubotaru, A.V. Chumak, Q. Wang, V.S. Tiberkevich, B. Hillebrands A.A. Serga. Commun. Phys. **3**, 17 (2020).
[9] X. Wang, H. Zhang, X. Wang. Phys.Rev. Appl. **9**, 2 (2018).
[10] A.V. Sadovnikov, E.N. Beginin, S.E. Sheshukova, D.V. Romanenko, Y.P. Sharaevskii, S.A. Nikitov. Appl. Phys. Lett., **107**, 202405 (2015).
[11] Q. Wang, P. Pirro, R. Verba, A. Slavin, B. Hillebrands, A.V. Chumak. Sci. Adv. **4**, e1701517 (2018).
[12] Y.K. Fetisov, G. Srinivasan. Appl. Phys. Lett. **88**, *14*, 143503 (2006).
[13] Y.K. Fetisov, G. Srinivasan. Appl. Phys. Lett. **93**, 033508 (2008).
[14] A.V. Sadovnikov, A.A. Grachev, S.E. Sheshukova, Y.P. Sharaevskii, A.A. Serdobintsev, D.M. Mitin, S.A. Nikitov. Phys. Rev. Lett. **120**, 257203 (2018).
[15] N.S. Gusev, A.V. Sadovnikov, O.G. Udalov. Phys. Rev. B **105**, 024405 (2022).
[16] N.S. Gusev, A.V. Sadovnikov, S.A. Nikitov, M.V. Sapozhnikov, O.G. Udalov. Phys. Rev. Lett. **124**, 157202 (2020).
[17] P.P. Silvester, R.L. Ferrari. Finite Elements for Electrical Engineers. Cambridge University Press (1996). 541 p.
[18] O.C. Zienkiewicz, R.L. Taylor, J.Z. Zhu. The finite element method: its basis and fundamentals. Elsevier (2005).
[19] A. Vansteenkiste, J. Leliaert, M. Dvornik, M. Helsen, F. Garcia-Sanchez, B. Van Waeyenberge. AIP Advances **4**, 107133 (2014).
[20] L.D. Landau, E.M. Lifshitz. Phys. Zs. Sow. **8**. P. 153–1935.
[21] T. Gilbert. Phys. Rev. **100**, 1243 (1955).
[22] A.V. Sadovnikov, E.N. Beginin, M.A. Morozova, Yu.P. Sharaevskii, S.V. Grishin, S.E. Sheshukova, S.A. Nikitov. Appl. Phys. Lett. **109**, 042407 (2016).

Editor T.N. Vasilevskaya